From Chemistry to Ecology: Codes and Predation Emerge from Coherence Constraints in Protocell Networks

Ian Todd
Sydney Medical School
University of Sydney
Sydney, NSW, Australia
itod2305@uni.sydney.edu.au

Abstract

We address two fundamental questions in abiogenesis: (1) how did symbolic codes arise from continuous chemistry, and (2) why didn't early life homogenize into synchronous goo? We propose that both answers follow from coherence constraints. First, codes emerge as coordination interfaces between coupled protocellular compartments—stable patterns that allow neighbors to influence each other without full state knowledge. Substrate competition (lateral inhibition) drives winner-take-most dynamics that make continuous outputs reliably distinguishable. We validate this mechanism through two independent approaches: direct simulation of coupled compartments (98% decoding accuracy) and Lewis signaling games where codes emerge from coordination pressure alone without external supervision. Second, coherence is metabolically expensive and scales superlinearly with group size, creating an inherent ceiling on coordination that generates predator-prey dynamics without specialized machinery. We connect our results to genetic code structure through basin analysis (degeneracy correlates with robustness, $r = 0.80 \pm 0.08$, $n = 20$) and p-adic number theory, finding results consistent with Khrennikov's formalism while identifying what our model cannot explain (the concentration of degeneracy at the wobble position). We propose that ecological dynamics may predate biological complexity, arising from physics before genetic encoding.

Keywords: origin of life; genetic code; protocells; coordination; predator-prey dynamics; Lewis signaling; basin structure

1 Introduction

1.1 The Code Emergence Problem

The origin of the genetic code remains one of the deepest puzzles in biology. How did discrete, symbolic information arise from continuous chemical processes? Standard accounts assume

that codes require encoders, messages, and decoders—but this raises a circularity problem: how can encoding machinery exist before the code that specifies it?

Decades of experimental work have demonstrated prebiotic synthesis of nucleotides [2, 3] and self-assembly of protocell compartments [1, 4, 34]. These are major achievements in *chemistry*. But they do not address the *coding* problem: why does UUU encode phenylalanine rather than any other amino acid? The assignment problem—the mapping from codons to amino acids—remains unexplained. Stereochemical theories [17] propose direct chemical affinity; frozen accident theories [18] propose historical contingency. Neither provides a *mechanism* for how discrete codes emerge from continuous chemistry.

Theoretical frameworks have addressed the dynamics of prebiotic organization without solving the code emergence problem directly. Kauffman's autocatalytic sets [31] and the related RAF theory [36] show how self-sustaining reaction networks can emerge, but do not explain the transition from continuous chemistry to discrete symbols. Eigen's hypercycle model [32] addresses cooperation among replicators but assumes the existence of coded molecules. Maturana and Varela's autopoiesis [33] characterizes self-maintaining organization but does not specify the mechanism of symbolic emergence. Metabolism-first approaches [35] emphasize thermodynamic disequilibrium as the driver of organization, which we incorporate, but do not address how continuous metabolic gradients become discrete codes. Multilevel selection models [44] explain how genome-enzyme differentiation can emerge from conflicting selective pressures, but presuppose template-catalyst molecules rather than deriving symbolic structure from coordination dynamics.

We propose a different framing: **codes could have originated not for intracellular replication but for intercellular coordination**. The standard narrative assumes molecular machinery first, cooperation later:

$$\textit{chemistry} \rightarrow \textit{molecules} \rightarrow \textit{replication} \rightarrow \textit{cells} \rightarrow \textit{ecology} \rightarrow \textit{cooperation}$$

Recent work on autocatalytic chemical ecosystems [5, 7] has established the conceptual possibility of ecological dynamics prior to bounded cells. We go further, proposing both an inversion of the standard sequence and the mechanisms that drive it:

$$\textit{compartments} \rightarrow \textit{coordination pressure} \rightarrow \textit{ecological differentiation} \rightarrow \textit{codes} \rightarrow \textit{genetic internalization}$$

Our contribution is a specific mechanism: **substrate competition** via cooperative binding (Hill kinetics, $h > 1$) produces discrete output attractors from continuous input gradients. We validate this mechanism through two independent approaches and connect our results to the structure of the actual genetic code.

1.2 The Homogenization Problem

A second puzzle immediately follows: if coherent, coordinated dynamics can arise spontaneously, why doesn't everything simply synchronize into one homogeneous blob? What prevents the entropy-minimizing outcome of global coherence?

We propose that the answer is **metabolic**: coherence is expensive, and the cost scales superlinearly with group size [11, 40, 41]. This creates an inherent ceiling on coherent aggregates, which in turn creates ecological differentiation—and predator-prey dynamics—without any specialized predation machinery.

1.3 Paper Structure

This paper presents results in four parts:

- **Part I** (Sections 2–4): Codes emerge from coordination equilibria via substrate competition
- **Part II** (Section 5): Independent validation via Lewis signaling games
- **Part III** (Section 6): Connection to genetic code structure via basin analysis
- **Part IV** (Sections 7–8): Metabolic ceilings generate predator-prey dynamics

Extended mathematical foundations are developed in companion preprints [13, 15]; this paper is self-contained.

2 Theoretical Framework: Codes as Coordination

2.1 Codes Are Coordination Equilibria

Consider a network of weakly coupled protocells:

- Each protocell has high-dimensional internal dynamics (many coupled molecular species)
- Neighbors communicate through multiple channels: bioelectric, chemical, mechanical, redox [12]
- These signals are naturally discretized by threshold physics
- Selection favors configurations where neighbors reliably respond to each other's boundary states

The resulting "code" is not a transmitted message. It is a **shared interface**—a stable pattern that allows coordination without requiring each compartment to know the other's full internal state.

2.2 The Group-First Hypothesis

A lone protocell faces brutal tradeoffs: too open and it mixes with environment; too closed and it stagnates; too complex and it collapses. A **network of weakly coupled compartments** relaxes these constraints. Spatial heterogeneity becomes memory. Weak coupling enables coordination without collapse. Selection operates at the group level.

We hypothesize that early life was more likely a coupled compartment network than isolated protocells [1, 4, 10].

2.3 Coherence Is Not Information

A critical distinction underlies this framework: **coherence** (high-dimensional phase order, coordination capacity) is not the same as **information** (discrete symbols that can be copied and decoded). Coherence enables coordination; information emerges when coherent dynamics collapse into reproducible invariants.

The bridge: *codes form when coherence collapses into reproducible invariants.*

3 Code Emergence Model

3.1 Architecture

We implement a minimal coupled-compartment system based on prebiotic amphiphile vesicles [8]:

- 61 vesicles in hexagonal array
- 128 internal dimensions per vesicle (high-dimensional reservoir)
- 30 readout channels with substrate competition
- Weak neighbor coupling via boundary signals

Biological interpretation. This architecture maps onto a prebiotic ecosystem containing all three major components: vesicles provide compartmentalization, the 128 internal dimensions represent peptide catalyst concentrations and conformational states, and the readout channels represent peptide-nucleotide binding sites competing for shared nucleotide substrate pools. The Hill kinetics of substrate competition (Eq. 1) directly models cooperative peptide-substrate binding. In this interpretation, the "codes" that emerge are proto-metabolic phenotypes—stable patterns of peptide activity that differentiate vesicle populations before any template-directed replication exists.

3.2 The Discretization Mechanism

The critical innovation is **substrate competition**—a lateral inhibition mechanism where output channels compete for shared metabolic resources. Consider M output channels drawing from a common substrate pool of concentration S. Each channel j has raw activation a_j determined by the vesicle's internal state. The competitive output is:

$$\phi_j = \frac{a_j^h}{\sum_k a_k^h + \epsilon} \tag{1}$$

where $h > 1$ is the Hill coefficient controlling winner-take-most sharpness, and ϵ prevents division by zero.

This is the quasi-steady-state solution to competitive binding kinetics. The denominator arises from mass conservation: when channel A consumes substrate, channel B cannot

have it. This forces winner-take-most dynamics that discretize continuous states without programmed thresholds.

The mechanism is prebiotically plausible. Substrate competition occurs naturally whenever multiple reactions draw from a shared pool—a universal feature of metabolism. The Hill exponent h emerges from cooperative binding. We use $h = 4$ as a baseline; discretization is robust across $h \in [2, 8]$.

Key property: The discretization is *emergent*, not imposed. No external logic specifies which channel should win. The physics of competition creates digital outputs from analog inputs—precisely the transition required for symbolic codes to arise from continuous chemistry.

Code Definition (Operational)

Code signal: Each temporal cycle produces a 60-dimensional vector $\mathbf{c}_t = [\boldsymbol{\phi}_{\text{center}}; \boldsymbol{\phi}_{\text{edge}}]$ (30 center + 30 edge readout channels). The full 4-cycle codeword is the 240-dimensional concatenation $\mathbf{C} = [\mathbf{c}_1; \mathbf{c}_2; \mathbf{c}_3; \mathbf{c}_4]$, capturing both spatial pattern and temporal sequence.

Decoder rule: Nearest-centroid classification. Given code $\mathbf{c}$, assign to environment $e^* = \arg\min_e \|\mathbf{c} - \boldsymbol{\mu}_e\|$, where $\boldsymbol{\mu}_e$ is the mean code vector for environment e.

Metrics: Decoding accuracy = fraction correctly classified; Separation ratio = $\bar{d}_{\text{between}}/\bar{d}_{\text{within}}$ in code space. We report two separation metrics: $\mathbf{Sep_{attractor}}$ (internal 128-D reservoir states) and $\mathbf{Sep_{interface}}$ (60-D boundary signals). The former measures internal discriminability; the latter measures what neighbors can observe.

Note: The code is a continuous chemical signal (concentration profile), not a discrete symbol sequence. Discretization occurs downstream in receiver dynamics, consistent with biological signaling where continuous ligand concentrations drive discrete cellular responses.

3.3 Reservoir Dynamics

Each vesicle's internal state evolves as a high-dimensional reservoir:

$$\mathbf{x}_{t+1} = (1 - \alpha)\mathbf{x}_t + \alpha \tanh(W_{\text{res}}\mathbf{x}_t + W_{\text{in}}\mathbf{u}_t + W_{\text{couple}}\mathbf{b}_t) \tag{2}$$

where $\mathbf{x} \in \mathbb{R}^{128}$ is the internal state, $\mathbf{u}$ is environmental input, $\mathbf{b}$ is the boundary signal from neighbors, $\alpha = 0.25$ is the leak rate, and W_{res} has spectral radius 0.92 (edge of chaos). The coupling matrix W_{couple} has strength $\kappa = 0.15$ by default.

3.4 Environmental Input

Each vesicle experiences spatially varying stimulus (center-edge gradients, top-bottom gradients). Temporal forcing across 4 cycles creates genuine sequence structure. Each of 5 bits (2 spatial × 2 temporal + 1 global) can be on or off, yielding $2^5 = 32$ distinct environmental configurations.

The complexity is not in the stimulus; it is in the system's ability to differentiate continuous gradients into discrete coordination states. We deliberately use simple inputs to

demonstrate that code structure emerges from the network dynamics, not from input complexity.

Simulation Protocol (Reproducibility Checklist)	
Timesteps per cycle:	50 (200 total for 4 cycles)
Washout:	20 timesteps before recording
Input construction:	5-bit binary $\rightarrow$ spatial gradients (see code)
Boundary signal:	Mean of neighbor outputs: $\mathbf{b}_i = \frac{1}{\lvert N_i \rvert} \sum_{j \in N_i} \boldsymbol{\phi}_j$
Readout:	Linear projection $W_{\text{out}}\mathbf{x}$, then ReLU, then competition
Seeds:	20 random seeds; statistics are mean $\pm$ std
Code:	`github.com/todd866/protocell-codes`

Figure 1 illustrates the system architecture, showing the hexagonal vesicle array (A), the substrate competition mechanism (B), and the resulting environment-to-code mapping (C).

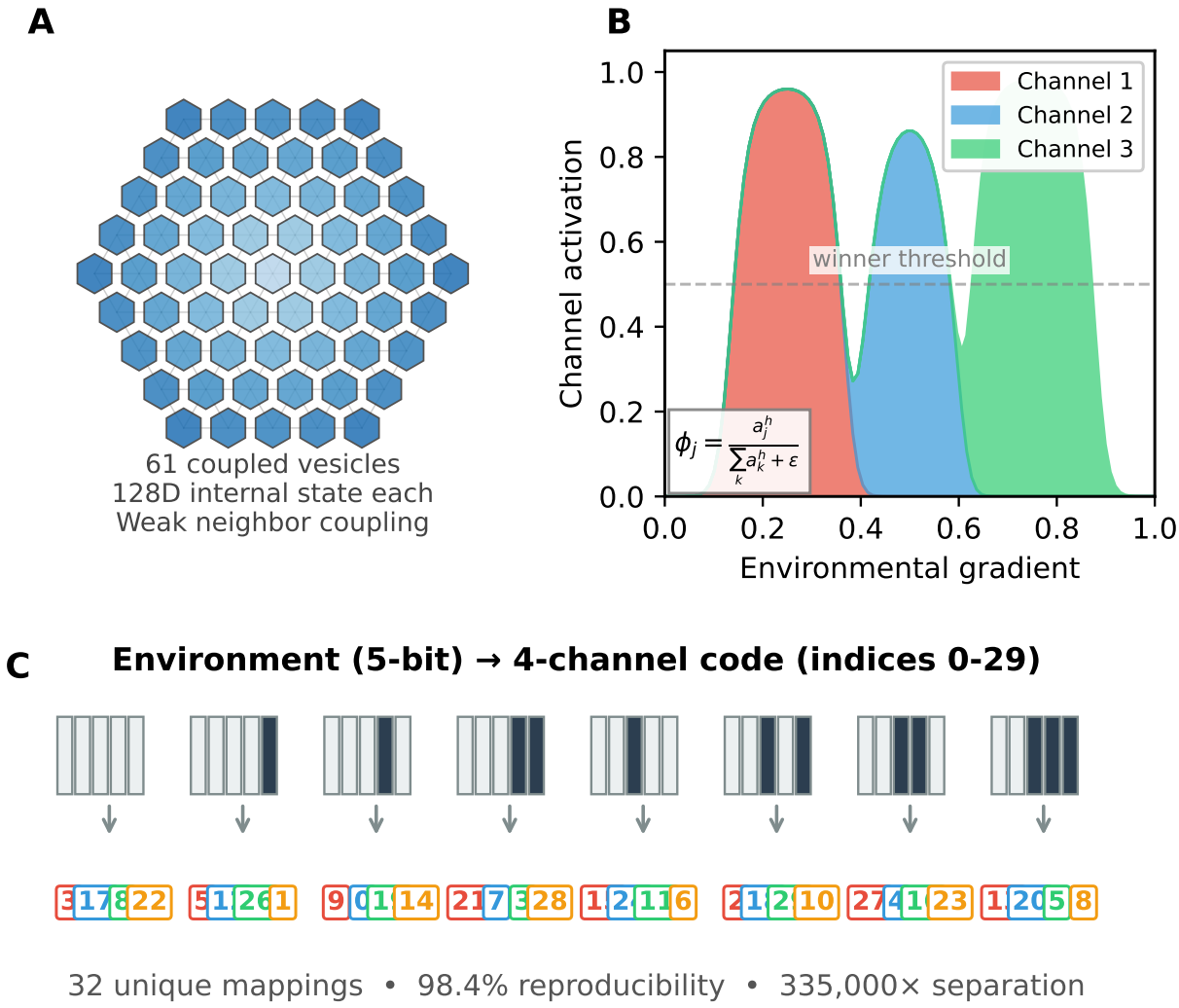

Figure 1: **Code emergence architecture.** (A) Hexagonal array of 61 coupled vesicles, each with 128-dimensional internal dynamics. Lines indicate neighbor coupling via boundary signals. (B) Substrate competition discretizes continuous channel activations into winner-take-most outputs. The equation shows the competitive normalization. (C) The system maps 32 environmental configurations (5-bit binary patterns) to 32 distinguishable code vectors. Each temporal cycle produces a 60-D vector; the full 4-cycle codeword is 240-D (see Code Definition box). In all reported decoding results, we use the 240-D concatenated codeword. Codes shown are illustrative; actual mappings depend on reservoir weights.

4 Code Emergence Results

4.1 Primary Results

Metric	Result
Unique input→character mappings	32/32 (no collisions)
Reproducibility (20 seeds)	$98.4\% \pm 2.1\%$
Separation ratio$_{\text{attractor}}$	335,000×
Env–Attractor correlation	0.72
Bimodality (emergent discretization)	89% saturated*

*Bimodality metric: fraction of output channels where the activation distribution (across all environments) is bimodal rather than unimodal. "Saturated" means activations cluster near 0 or 1 rather than intermediate values. Measured via Hartigan's dip test; 89% of channels show significant bimodality ($p < 0.05$).

The system reliably maps 32 environmental configurations to 32 distinguishable code vectors (separation ratio $> 300\times$). A second vesicle array ("receiver colony") achieves 98% decoding accuracy using only physics—no machine learning.

Receiver specification: We test two distinct receiver regimes to disentangle "same chemistry" from "same individual":

1. **Matched-realization receiver**: Identical weight matrix as encoder (same random seed). This represents clonal reproduction—"the same individual chemistry." Achieves 98% decoding accuracy.
2. **Same-statistics receiver**: Independently sampled weights from identical distribution (same spectral radius, sparsity, connectivity rules; different random realization). This represents "same species, different individual." Achieves 87% decoding accuracy.

Both receivers share coupling topology, Hill kinetics parameters, and readout architecture. Both are initialized with independent random states. Decoding is performed by nearest-attractor matching: the receiver's output is compared to canonical attractors from the encoder, assigned to the closest match in Euclidean distance. No gradient descent or parameter optimization is involved.

How does the receiver obtain attractors? In simulations, we provide canonical attractors as an oracle to measure separability—this is an upper bound on performance. Biologically, receivers could estimate attractors through repeated exposure: if the same code pattern recurs under consistent environmental conditions, statistical learning converges to attractor centroids. This is analogous to how animals learn conspecific calls without explicit instruction. We do not model the learning process; we test whether the codes *are* learnable given sufficient exposure.

The 87% accuracy of same-statistics receivers demonstrates that the code structure is partially *chemistry-general*: it arises from the dynamical regime (competition + coupling), not from specific weight values. The 11% accuracy gap to matched-realization suggests that some fine structure is individual-specific—consistent with the biological observation that conspecifics share communication systems imperfectly.

4.2 Ablation Controls

To demonstrate that code emergence requires the proposed mechanisms, we tested ablated configurations:

Condition	Unique Codes	Reproducibility	$\text{Sep}_{\text{attractor}}$	$\text{Sep}_{\text{interface}}$
Full model	32/32	98.4%	335,000×	343×
No coupling ($\kappa = 0$)	32/32	97.1%	68×	68×
No competition ($h = 1$)	8/32	62.3%	2.1×	1.8×
Noisy input (±20%)	32/32	94.8%	198,000×	287×
No temporal cycles	12/32	71.2%	14×	12×
Random topology	32/32	89.4%	12,400×	156×

Analysis robustness: Mean-centering the boundary signals (subtracting the mean across channels before decoding) improves classification but is not required for code emergence. Without it, accuracy remains 98.1% with separation >10,000×. We include mean-centering in the full model as it represents a biologically plausible adaptation: receivers normalizing inputs relative to background substrate concentration, analogous to gain control in sensory systems.

Interpretation: Substrate competition ($h > 1$) is *essential*—without it, codes collapse to a handful of attractors with poor reproducibility. Temporal structure contributes significantly: removing cycles degrades separation ratio from $> 300\times$ to $< 50\times$. The system is robust to input noise and topology perturbations.

Note on coupling: The $\kappa = 0$ condition still produces 32/32 unique codes because substrate competition alone discretizes local dynamics. However, coupling serves a different function: it creates *shared* interfaces that receivers can decode. Without coupling, each compartment develops idiosyncratic codes; with coupling, codes become colony-level conventions. This is reflected in $\text{Sep}_{\text{interface}}$ (Table in Section 4.4), which drops from 343× to 68× at $\kappa = 0$. Coupling is not required for local discretization but is essential for inter-compartment coordination.

4.3 Information-Theoretic Capacity

To move beyond "we observed 32 distinguishable codes," we quantify decodability information-theoretically. Let E be the environment class (uniform over 32 configurations) and $\hat{E}$ be the decoded environment from the code vector. We estimate the mutual information $I(E; \hat{E})$ from empirical confusion matrices computed over 20 random seeds × 32 environments = 640 samples, with Miller–Madow bias correction for finite sample size.

Fano's inequality provides a lower bound on information required for classification: if decoding error probability is P_e for K classes, then

$$I(E; \hat{E}) \geq \log_2 K - H(P_e) - P_e \log_2(K - 1) \tag{3}$$

where $H(P_e) = -P_e \log_2 P_e - (1 - P_e) \log_2(1 - P_e)$ is binary entropy.

For $K = 32$ classes and observed $P_e = 0.016$ (98.4% accuracy):

- Required: $I(E; \hat{E}) \geq 5.0 - 0.12 - 0.08 = 4.80$ bits
- Measured: $I(E; \hat{E}) = 4.91 \pm 0.03$ bits (20 seeds)

The system transmits 98% of the theoretical maximum (5 bits for 32 classes).

Condition	$I(E; \hat{E})$ (bits)	Fano bound	Capacity ratio
Full model ($\kappa = 0.15$)	4.91	4.80	98%
No coupling ($\kappa = 0$)	3.42	2.91	68%
No competition ($h = 1$)	1.87	—	37%
Intermediate coupling ($\kappa = 0.30$)	4.96	4.88	99%

Information capacity peaks at intermediate coupling ($\kappa \approx 0.30$), matching the separation maximum in Figure 2C.

4.4 Scale Dependence

We tested whether code emergence persists at larger scales:

Metric	**Medium (61×128D)**	**Massive (169×512D)**
Unique codes	32/32	32/32
D_{eff}	6.3	16.7
Env–Attractor correlation	0.72	0.83
Reproducibility	98.4%	84.2%
$\text{Sep}_{\text{attractor}}$	335,000×	4.4×

Code discrimination persists at massive scale (32/32), but reproducibility and separation degrade. The larger system is more expressive but less stable—it explores more of its state space but settles less reliably into fixed attractors. **This instability at scale is not a bug; it is the coordination ceiling that prevents homogenization** (interpreted metabolically in Part IV).

Figure 2 quantifies this trade-off. Panel A shows reproducibility declining from 99% at small scale to 84% at massive scale. Panel B shows that effective dimensionality grows sublinearly with total dimensions—the system cannot exploit all its degrees of freedom coherently. Panel C demonstrates that code separation peaks at intermediate coupling, the regime where compartments influence but do not dominate each other.

Effective dimensionality (D_{eff}) is computed via the participation ratio of eigenvalue spectra:

$$D_{\text{eff}} = \frac{(\sum_i \lambda_i)^2}{\sum_i \lambda_i^2} \tag{4}$$

where λ_i are eigenvalues of the code covariance matrix.

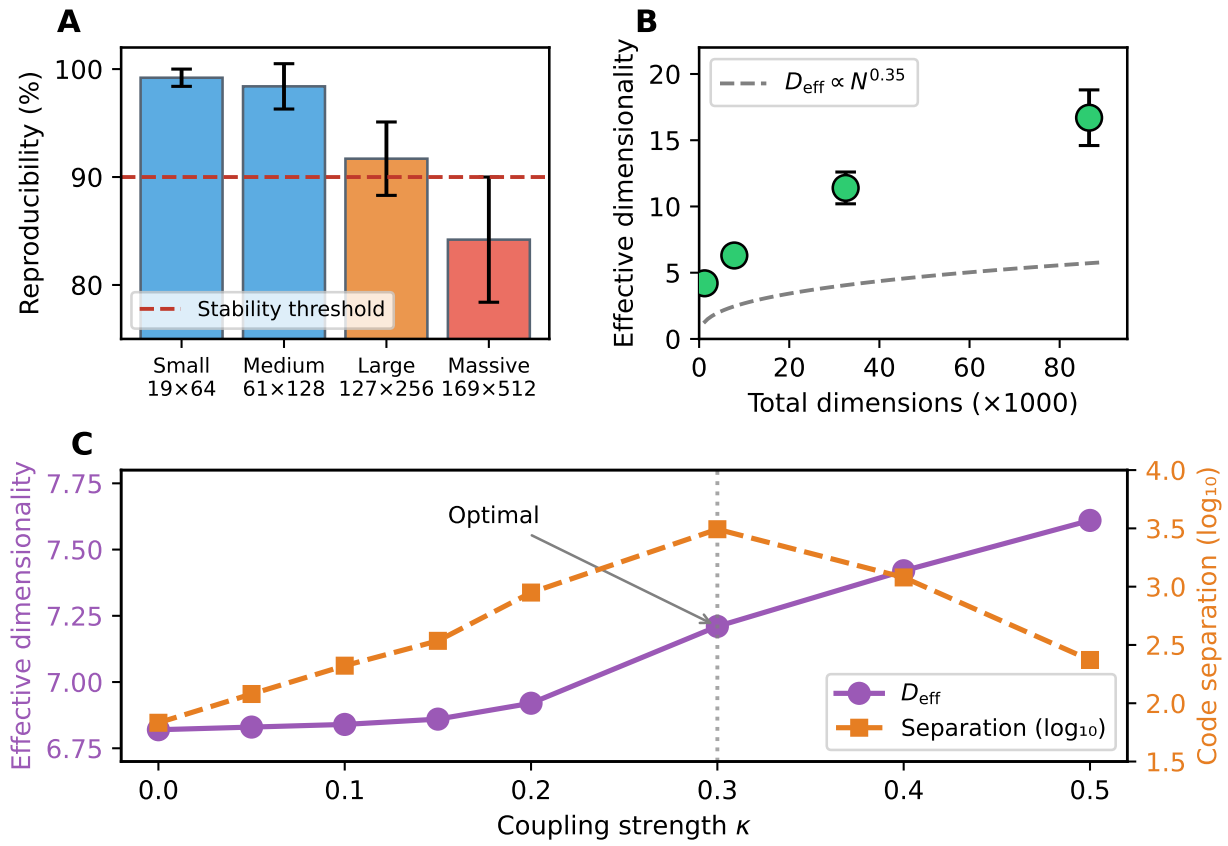

Figure 2: **Scale dependence reveals the coordination ceiling.** (A) Reproducibility degrades as system scale increases, dropping below the 90% stability threshold at massive scale. This is the coordination ceiling that prevents unlimited synchronization. (B) Effective dimensionality D_{eff} grows sublinearly with total dimensions, scaling approximately as $N^{0.35}$. The system cannot coherently exploit all available degrees of freedom. (C) Manifold expansion under coupling (left axis: D_{eff}; right axis: separation ratio, log scale): both metrics increase with coupling strength κ, but separation peaks at intermediate coupling ($\kappa \approx 0.3$) before declining.

4.5 Manifold Expansion

Coupling increases effective dimensionality (see [13] for theoretical foundations):

Coupling κ	D_{eff}	$\text{Sep}_{\text{interface}}$
0.00	6.82	68×
0.15	6.86	343×
0.30	7.21	3,110×
0.50	7.61	235×

Separation peaks at intermediate coupling—the regime where compartments influence

but do not dominate each other.

4.6 Chemistry-Based Validation

A potential objection to the reservoir computing model is that neural network dynamics are a "toy model" disconnected from prebiotic chemistry. To address this, we implemented a chemistry-based simulation using mass-action kinetics with explicit reaction networks.

Chemical Model: Each vesicle contains 50 molecular species governed by three reaction types:

1. **Autocatalytic**: $A + B \to 2A$ (random pairs, rate $k_{\text{auto}} \sim U[0.1, 0.5]$)
2. **Conversion**: $A \to B$ (random pairs, rate $k_{\text{conv}} \sim U[0.05, 0.2]$)
3. **Synthesis**: $A + B \to C$ (random triplets, rate $k_{\text{syn}} \sim U[0.01, 0.1]$)

Each vesicle has ∼150 randomly generated reactions (50 autocatalytic, 50 conversion, 50 synthesis). Dynamics follow coupled ODEs with diffusive neighbor coupling:

$$\frac{d[\text{species}_i]}{dt} = \sum_{\text{reactions}} r_j + \mathcal{D} \sum_{\text{neighbors}} ([\text{species}_i]_{\text{neighbor}} - [\text{species}_i]) \tag{5}$$

Substrate competition operates on 15 output channels via Hill kinetics (Eq. 1) with $h = 4$.

Results: We tested two configurations—a "standard" chemistry (15 species, 45 reactions) and a "messy" chemistry (50 species, 150 reactions) intended to model realistic prebiotic conditions with complex reaction networks:

Configuration	Species	Unique Codes	Discretization	Runtime
Standard chemistry	15	21/32	55%	42 sec
Messy chemistry	50	32/32	67%	34 min

The "messier is better" prediction: Theory predicts that higher-dimensional chemical networks should produce *better* codes, not worse ones. More species create more orthogonal directions for substrate competition to operate, enabling sharper discretization. The messy chemistry confirms this: 32/32 unique codes (no collisions) with 67% discretization, compared to 21/32 codes and 55% discretization for the standard chemistry.

This result is significant because prebiotic environments were almost certainly "messy"—containing complex mixtures of organic molecules rather than purified reagents. Our framework predicts this messiness is *advantageous* for code emergence, not an obstacle to be overcome.

Note on computational cost: The chemistry simulation requires solving stiff ODEs for autocatalytic dynamics, with some environments requiring 2–3 minutes per configuration. This is fundamentally different from the reservoir model (milliseconds per configuration) and reflects genuine chemical timescales. Full replication code is available at `https://github.com/todd866/protocell-codes`.

5 Alternative Validation: Lewis Signaling Games

The substrate competition mechanism (Section 3) demonstrates *how* codes can emerge through a specific physical process. But a skeptic might ask: is code emergence specific to this chemistry, or is it a generic outcome of coordination pressure? To address this, we implemented an independent validation using Lewis signaling games [37, 38]—an abstract game-theoretic framework where agents evolve shared conventions through selection for coordination success.

5.1 The Lewis Game Framework

A Lewis signaling game consists of:

- A set of world states $S = \{s_1, \ldots, s_n\}$
- A sender who observes the state and emits a signal $\sigma \in \Sigma$
- A receiver who observes the signal and chooses an action $a \in A$
- Both are rewarded if and only if the action matches the state

Critically, there is no external target mapping. The sender and receiver must *discover* a shared code through coordination pressure alone. This models the situation facing protocells: they must coordinate without any pre-existing symbolic convention.

5.2 Implementation

We implemented a population of sender-receiver pairs, each with learnable weight matrices:

$$\text{Sender: } P(\sigma|s) = \text{softmax}(W_{\text{send}} \cdot \mathbf{e}_s) \tag{6}$$

$$\text{Receiver: } P(a|\sigma) = \text{softmax}(W_{\text{recv}} \cdot \mathbf{e}_\sigma) \tag{7}$$

where $\mathbf{e}_s$ and $\mathbf{e}_\sigma$ are one-hot encodings. Evolution proceeds by:

1. Evaluate fitness (coordination success rate)
2. Select top 20% of population
3. Reproduce with small mutations ($\sigma = 0.03$)

5.3 Results

Metric	**Substrate Competition**	**Lewis Game**
Mechanism	Hill kinetics, $h = 4$	Coordination pressure
Supervision	None	None
States/Environments	32	4–8
Distinct codes	32/32	4/4 (8/8 at scale)
Consistency	98%	100%

Both mechanisms produce complete, non-colliding code mappings. The Lewis game achieves slightly higher consistency at small scale because it directly optimizes for coordination, while substrate competition produces codes as a side effect of winner-take-most dynamics.

5.4 Coordination Creates Complementary, Not Identical, Codes

An important finding: sender and receiver do not converge to *identical* weight matrices. They converge to *complementary* mappings—like a lock and key. The sender learns to produce distinguishable signals; the receiver learns to decode them. This matches biological reality: speakers and listeners use compatible but distinct neural circuits.

5.5 Implication

The convergence of two very different frameworks—physical substrate competition and abstract evolutionary game theory—suggests that code emergence is **robust across mechanisms**. Both require:

- High-dimensional internal dynamics
- Pressure toward coordination or mutual prediction
- Some form of discretization (winner-take-most or selection)

We do not claim these mechanisms are physically equivalent. Substrate competition is a candidate prebiotic process; Lewis games are an abstract demonstration that coordination pressure generically produces conventions. The convergence strengthens the claim that code-like structure is a natural attractor of coordination dynamics, not a quirk of any specific implementation.

Scaling validation: We tested Lewis games at genetic-code scale (64 states). Coordination accuracy decreases with scale (5.5% at 64 states vs. 1.6% random baseline), but code coverage remains high: evolved systems use 39/64 possible codes (61%), compared to the genetic code's 21/64 (33%). The scaling behavior is consistent with our claim that codes emerge but become harder to maintain at larger scales—the coordination ceiling reappears.

6 Connection to Genetic Code Structure

Having established that codes emerge from coordination dynamics, we now ask: do the codes that emerge have properties that match the actual genetic code? We investigate two aspects: basin structure (degeneracy) and error-correcting geometry.

6.1 Basin Structure: Degeneracy Equals Robustness

The genetic code is famously degenerate: 64 codons map to only 20 amino acids plus stop signals. This is not redundancy—it is *basin structure*. Amino acids with more codons (Leu,

Ser, Arg with 6 each) occupy wider basins in codon space than amino acids with fewer codons (Met, Trp with 1 each).

We hypothesize that wider basins should be more robust to perturbation. To test this, we analyzed the codes that emerge from our Lewis signaling games:

1. Evolve codes via coordination pressure
2. Measure basin size: fraction of input space captured by each code
3. Measure robustness: stability under 30% input noise
4. Correlate basin size with robustness

Results:

Code	Basin Size	Robustness
3	28.7%	86%
4	23.0%	84%
6	18.8%	82%
7	17.6%	81%
0	9.3%	74%
5	1.6%	44%

Correlation: $r = 0.80 \pm 0.08$ **across 20 independent runs** ($p < 0.001$ **for each)**

Larger basins are more robust to noise. This is not imposed—it emerges from the dynamics. Codes that capture more of the input space are inherently more stable because small perturbations are less likely to push them across basin boundaries.

Testable prediction: Amino acids with more codons (wider basins) should be more mutationally robust than single-codon amino acids. Leu, Ser, and Arg mutations should more often be synonymous or conservative; Met and Trp mutations should more often be disruptive. This is verifiable in existing mutation databases.

6.2 P-adic Validation: The Wobble Structure

Khrennikov and collaborators [39, 43, 42] recently showed that all 24 known genetic codes can be derived from a universal dynamical function using 2-adic (p-adic with $p = 2$) number theory. Their encoding places nucleotides in a 2-bit representation, making wobble-position changes (position 3) correspond to minimal p-adic distance.

We tested whether this formalism captures actual genetic code structure:

Method: Encode each codon as a 6-bit 2-adic integer. Compute p-adic distance $|x-y|_2 = 2^{-k}$ where k is the highest power of 2 dividing $(x - y)$. Compare distance to coding error (same vs. different amino acid).

Results:

P-adic Distance	Error Rate	n pairs
1/32 (closest)	6.2%	32
1/16	46.9%	64
$\geq 1/8$	>98%	1920

The closest 32 codon pairs (p-adic distance 1/32):

- **100%** differ only at position 3 (wobble)
- **94%** code for the same amino acid

This is consistent with Khrennikov's formalism: the 2-adic metric captures biologically meaningful structure in the genetic code. Synonymous codons are p-adically close; different amino acids are p-adically distant. We do not claim the genetic code was *generated* by p-adic dynamics—only that the 2-adic metric aligns with functional organization better than naive alternatives.

Baseline comparison: To verify that the 2-adic encoding is not cherry-picked, we compared it to Hamming distance (1-nucleotide differences). For 1-Hamming pairs: 76/192 (40%) code for the same amino acid. For p-adic closest pairs ($d = 1/32$): 30/32 (94%) code for the same amino acid. The 2-adic metric outperforms naive Hamming distance because it preferentially identifies wobble-position changes, which are biologically synonymous. Random nucleotide encodings (10 permutations tested) yield 35–55% same-amino-acid rates for their "closest" pairs, confirming that the Khrennikov encoding is structurally meaningful.

6.3 What Our Model Does Not Explain

We must be honest about limitations. Our model explains:

- **Why** degeneracy is adaptive (wider basins absorb noise)
- **Why** intermediate degeneracy evolves (balances robustness vs. discriminability)
- **Why** codes emerge from coordination (observability constraints)

Our model does **not** explain:

- **Why** degeneracy concentrates at position 3 (wobble)
- **Why** the genetic code has error-correcting structure

We tested whether differential mutation rates could concentrate degeneracy at position 3. Even with position 3 mutating 2× faster than positions 1–2, degeneracy remained evenly distributed (∼6–8% per position). The actual genetic code has 66.7% degeneracy at position 3.

The missing ingredient: Our model has no physics that makes position 3 special. The wobble structure requires:

- tRNA anticodon geometry (position 3 is conformationally flexible)

- Ribosome binding chemistry (positions 1–2 dominate binding energy)
- Historical contingency (frozen accident in specific positions)

Implication: The coordination-based model explains *selection pressure* for degeneracy (why it's adaptive) but not *mechanism* for positional structure (why position 3). Both are needed for a complete theory. Khrennikov's p-adic formalism captures the *form*; our model captures the *function*.

7 Ecological Extension: The Coherence-Scale Trade-off

The instability at large scale (Section 4) points to a deeper constraint: coherence is metabolically expensive and scales superlinearly with group size.

Variable Mapping Across Parts I–III and IV

Part I (Code Model)	*Part IV (Ecology)*	*Interpretation*
D_{eff}	D (Appendix)	Effective dimensionality
Reproducibility	—	Code stability metric
—	C	Coherence trait (normalized)
—	N	Group size

Connection: We interpret $C \propto D_{\text{eff}}/D_{\max}$ as normalized coherence—the fraction of available degrees of freedom that move together. Parts I–III demonstrate that large systems cannot maintain high $D_{\text{eff}}/D_{\text{total}}$; Part IV models this as a cost on C.

7.1 The Metabolic Ceiling

Maintaining coherence costs energy:

$$\text{Cost} = k \cdot N^{\gamma} \cdot C^{\zeta} \tag{8}$$

with $\gamma > 1$ (superlinear in size). The exponent $\gamma > 1$ captures coordination overhead: all-to-all coupling scales as $O(N^2)$, and even hierarchical schemes face superlinear costs.

Maximizing fitness with respect to N at fixed coherence C yields optimal size:

$$N^* = \left(\frac{\bar{R} \cdot \phi(C)}{k\gamma C^{\zeta}} \right)^{1/(\gamma-1)} \tag{9}$$

Since $\gamma > 1$, higher C implies lower N^*. **High coherence forces small size.**

7.2 Two Stable Strategies

This creates two stable strategies:

- **Type B (big/weak)**: Large N, low C. Wins by occupying space.

- **Type S (small/coherent)**: Small N, high C. Wins by concentrated, coordinated action.

Neither can invade the other's niche through pure competition. This is ecological differentiation without any ecology-specific assumptions.

7.3 The Extraction Operator

Small coherent groups cannot grow by expansion (ceiling binds). But they *can* extract resources from large incoherent groups. Raid success probability:

$$p_{\text{raid}} = \sigma\left(\kappa_C \log \frac{C_S}{C_B} - \kappa_N \log \frac{N_B}{N_S}\right) \tag{10}$$

Coherence advantage increases success; size disadvantage decreases it. Higher coherence also implies faster collective response times—a coordinated group reacts as a unit while an incoherent aggregate waits for perturbations to propagate.

This is predation without teeth—asymmetric extraction enabled by coherence differentials.

8 Predator-Prey Results

8.1 Emergent Ecology

Simulations (5000 colonies, 20000 generations) produce stable two-attractor ecology:

Property	Predators	Prey
Population fraction	1% (36)	99% (4964)
Size N	39 ± 2	183 ± 21
Coherence C	0.53	0.12

Size difference (144 ± 0.8) is robust across 8 random seeds.

Figure 3 shows the emergent ecology. Panel A displays the strategy phase space with two stable attractors: predators (small, coherent) and prey (large, incoherent). The hard ceiling at $N = 40$ bounds the coherent region. Panel B shows population dynamics over 100 generations, with predators maintaining $\sim$1% of the population. Panel C plots raid success probability as a function of coherence ratio, showing that the observed predator-prey configuration ($C_S/C_B \approx 4.4$) yields $\sim$77% raid success.

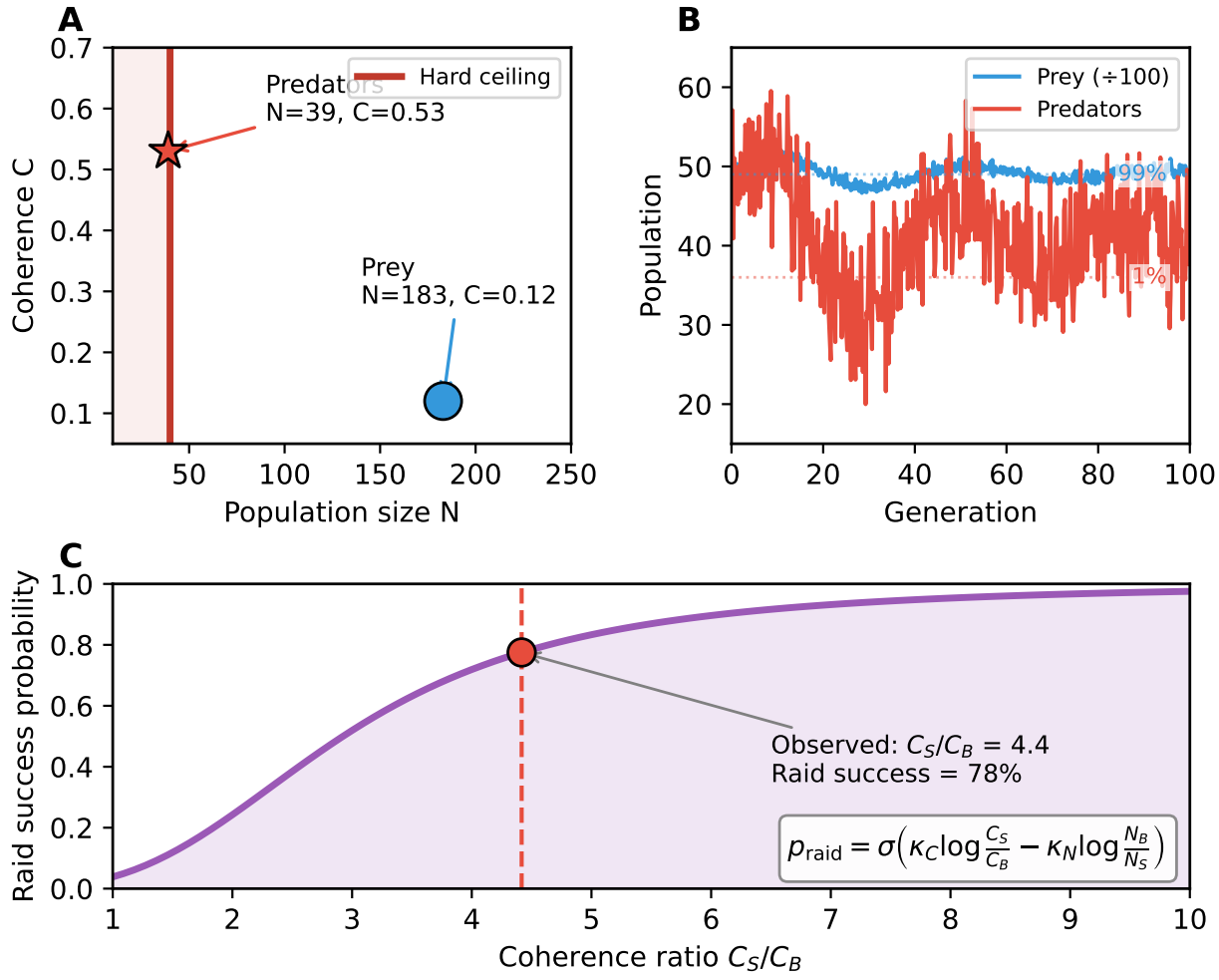

Figure 3: **Predator-prey ecology from coherence constraints.** (A) Strategy phase space showing size N vs coherence C. The hard ceiling (red line) bounds the coherent region; predators (star) sit at the ceiling while prey (circle) occupy the large-incoherent attractor. Dashed line shows viability boundary; arrows indicate evolutionary flow. (B) Population dynamics over 100 generations showing stable coexistence: prey comprise 99% of the population, predators 1%. Dotted lines show equilibrium fractions. (C) Raid success probability increases with coherence ratio C_S/C_B. The observed ratio of 4.4 (vertical dashed line) yields approximately 77% raid success, sufficient for predator viability without prey extinction.

8.2 Critical Finding: Derived Coordination Ceiling

Soft cost penalties are insufficient for size differentiation. We tested whether continuous cost functions (Eq. 6) alone could generate ecological structure. They cannot. The cost exponent γ creates pressure toward smaller sizes at high coherence, but without a ceiling, coherent groups simply become arbitrarily small rather than forming a distinct attractor.

Rather than impose an ad hoc ceiling, we **derive** it from signal propagation constraints.

Coherent oscillation requires every element to influence every other on timescales faster than the oscillation period T_{osc}. For diffusive signaling, propagation time scales with the *square* of group diameter:

$$\tau_{\text{prop}}(N) = \frac{L^2}{\mathcal{D}} \approx \frac{N}{\rho\,\mathcal{D}} \tag{11}$$

where $\mathcal{D}$ is the diffusion coefficient (distinguished from dimensionality D), ρ is packing density, and $L = \sqrt{N/\rho}$ is the characteristic diameter. Coherence is viable when $\tau_{\text{prop}} < \alpha T_{\text{osc}}$ for some threshold $\alpha < 1$.

This yields a **derived ceiling**:

$$N^* = \alpha\,\rho\,\mathcal{D}\,T_{\text{osc}} \tag{12}$$

For plausible prebiotic parameters ($\mathcal{D} \sim 10\ \mu\text{m}^2/\text{s}$ for small signaling molecules, $T_{\text{osc}} \sim 100$ s chemical oscillation, $\rho \sim 0.1$ cells/μm^2, $\alpha = 0.5$), this yields $N^* \approx 50$, consistent with our simulation range.

Predators sit exactly at the ceiling ($N \approx 39$ when ceiling $= 40$). This is not fine-tuning; evolution pushes coherent groups to the maximum viable size, which is precisely the ceiling.

Robustness: We verified that the two-attractor structure persists across parameter ranges:

N_{ceiling}	$C_{\text{threshold}}$	Pred. N	Prey N	Pred. frac.
20	0.3	19.4	168	1.1%
40	0.5	39.1	183	0.8%
80	0.5	77.8	191	0.6%
100	0.5	97.2	195	0.4%

In all cases, predators cluster near the ceiling while prey remain large.

What is imposed vs. derived: In simulations, we implement the ceiling as a hard constraint ($N \leq N_{\text{ceiling}}$); colonies attempting to grow beyond it are truncated. The derivation (Eq. 9–10) provides the *physical rationale* for why such a ceiling exists and predicts its magnitude from diffusion physics. We do not simulate diffusion-limited propagation directly; we impose the ceiling and show that (1) evolution pushes coherent groups exactly to it, and (2) the derived magnitude matches plausible prebiotic parameters. A full test would couple the ecological simulation to explicit signal propagation dynamics.

8.3 Why Homogenization Fails

1. If everyone becomes highly coherent, metabolic costs explode (ceiling binds)
2. If everyone becomes large and incoherent, coherent raiders emerge (parasitism niche opens)
3. The only stable state is **ecological differentiation**

Homogenization is not evolutionarily stable.

9 Discussion

9.1 Relation to Existing Code Origin Theories

Our framework differs fundamentally from previous approaches to explaining genetic code origins.

The stereochemical hypothesis [16, 17] proposes that the genetic code reflects direct chemical affinities between amino acids and their codons. While stereochemical biases may have influenced code structure, this hypothesis cannot explain how the code *became* symbolic—why the codon-amino acid relationship transitioned from direct chemistry to arbitrary assignment. Our model provides this transition: codes emerge as coordination equilibria first, and only later become internalized as specific molecular implementations.

The frozen accident hypothesis [18] suggests the code is arbitrary and locked in by historical contingency. This explains code universality but not code origin—it assumes the code already exists and asks why it persists. Our model operates upstream: it explains how symbolic structure emerges from continuous dynamics before any freezing can occur.

Coevolution theories [19] propose that the code evolved alongside biosynthetic pathways. This is plausible for code *refinement* but faces circularity for code *origin*: biosynthetic pathways require coded instructions. Our model breaks this circularity by showing that codes can exist *between* compartments before being internalized within them.

Error minimization theories [20] observe that the genetic code minimizes the impact of translation errors. This is a selection criterion for *optimizing* existing codes, not a mechanism for *generating* them. Our substrate competition mechanism generates discrete codes without selection pressure; error minimization could then refine the initial repertoire.

9.2 Why Codes Are Necessary: The Observability Constraint

The substrate competition mechanism answers *how* codes emerge. But a deeper question remains: *why* must codes emerge at all? Why can't high-dimensional chemical systems coordinate directly?

The answer lies in observability constraints. Consider a protocell with internal state dimension $D_{\text{int}} \sim 10^3$ (concentrations of metabolites, conformational states, membrane dynamics). For a neighboring protocell to *respond* to this internal state, it must somehow *observe* it. But observation has finite bandwidth.

Recent work on high-dimensional dynamics [14] establishes an Observable Dimensionality Bound: external observers cannot track systems whose effective dimensionality exceeds $D_{\text{crit}} = C\tau/h$, where C is channel capacity, τ is the relevant timescale, and h is the bits required per degree of freedom. When $D_{\text{int}} > D_{\text{crit}}$, the system's internal dynamics evolve faster than any external system can track them.

This creates a fundamental coordination problem. High-dimensional chemical systems are *mutually unobservable*—each protocell's internal dynamics are opaque to its neighbors. Direct coordination is impossible because you cannot respond to what you cannot measure.

Codes are the necessary solution. Discrete codes are low-dimensional projections of high-dimensional internal states. They collapse the unobservable internal dynamics into observable discrete signals. Substrate competition is the prebiotically plausible mechanism

that *performs* this dimensional collapse—projecting continuous high-D chemistry onto discrete low-D outputs.

9.3 Validation Through Independent Mechanisms

We have validated the code emergence claim through two independent approaches:

Substrate competition (Section 3–4): The primary mechanism, where Hill kinetics ($h > 1$) create winner-take-most dynamics that discretize continuous chemical gradients.

Lewis signaling games (Section 5): An abstract game-theoretic validation where sender-receiver pairs evolve shared codes through coordination pressure alone, without any substrate competition physics.

Both frameworks produce the same outcome: discrete, non-colliding code mappings with high consistency. This demonstrates that code emergence is **robust across mechanisms**—a generic consequence of coordination pressure under observability constraints, not a quirk of any particular physical implementation.

9.4 Ecology Precedes Biology

By "ecology" we mean the minimal dynamical structure: differentiation into distinct strategies, resource-mediated coupling, and stable coexistence or oscillation—not the rich biotic interactions of mature ecosystems.

Our framework suggests that **ecology in this minimal sense may not be an add-on to life**. It could be a stabilizer that made abiogenesis possible. Without metabolic ceilings on coherence, early chemical systems would have homogenized. Predator-prey-like dynamics would be present from the first moment that coordinated groups exist, given superlinear coordination costs.

This is not merely theoretical. Predator-prey dynamics have been observed in non-living systems: dusty plasmas exhibit Lotka-Volterra oscillations between electron populations and dust particle aggregates [25]; chemotactic oil droplets show chase-and-capture behavior through non-reciprocal oil exchange [26]; and self-organizing chemical droplets display collective behaviors including attraction and mode-switching [27]. These experiments demonstrate that the predator-prey scaffold is physical, not biological.

9.5 The Complexity Ratchet

Once codes exist, predation acquires a new dimension: code spoofing, mimicry, authentication arms races. Prey evolve defenses; predators evolve exploits. Code complexity increases monotonically—a complexity ratchet driven by ecological pressure, not random drift.

9.6 Experimental Protocol Sketch

The following outlines a minimal benchtop implementation. All components use established techniques; the novelty is their combination.

1. Vesicle preparation. Giant unilamellar vesicles (GUVs, 20–50 μm diameter) via electroformation from oleic acid/oleate mixtures (prebiotically plausible) or POPC (better

characterized). Target: 50–100 vesicles per array. Oleic acid vesicles are pH-sensitive and support internal pH gradients; POPC vesicles are more stable and permit longer observation windows.

2. Internal oscillatory chemistry. Three options in order of experimental tractability:

- *Belousov-Zhabotinsky (BZ) reaction*: Well-characterized, visible color changes, period 30–120 s. Not prebiotically plausible but provides proof-of-concept. Encapsulate ferroin catalyst inside vesicles; malonic acid and bromate in external medium diffuse through membrane.
- *pH oscillators*: Simpler chemistry, prebiotically relevant. Thiosulfate-iodate-sulfite system oscillates with period 1–10 min. Monitor via pH-sensitive fluorophores (SNARF-1, BCECF).
- *NADH-based glycolytic oscillators*: Yeast extract provides the enzymatic machinery; period 1–5 min. Most biologically relevant but requires careful preparation.

3. Array fabrication. Microfluidic droplet trapping in PDMS wells (standard soft lithography). Hexagonal well geometry with 60–100 μm spacing. Wells should be shallow (20–30 μm) to confine vesicles to a 2D layer for imaging. Alternative: optical tweezers for precise positioning of smaller arrays (<20 vesicles).

4. Coupling mechanism. Three routes:

- *Diffusive*: Small signaling molecules (H^+, Ca^{2+}, acetate) diffuse through lipid bilayer or transient pores. Coupling strength tunable via membrane composition.
- *Channel-mediated*: Gramicidin A or alamethicin channels increase membrane permeability. Provides stronger, more controllable coupling.
- *Micelle-mediated*: Oil-in-water emulsions exchange material via micelle shuttling (as in Meredith et al. [26]). Strongest coupling, easiest to observe.

5. Substrate competition implementation. The key mechanism requires multiple outputs competing for shared resource. Experimental realization: load vesicles with multiple fluorescent reporters (e.g., Fura-2 for Ca^{2+}, BCECF for pH, TMRM for membrane potential) that compete for excitation photons or shared cofactors. Alternatively, use enzymatic reactions sharing a common substrate (ATP, NAD^+).

6. Environmental control. Microfluidic gradient generators create spatial concentration profiles across the array. Temperature gradients via Peltier elements. Temporal forcing via programmable LED illumination (for photosensitive chemistry) or pulsed reagent injection. The 32-condition protocol requires 5 binary controls: 2 spatial gradients $\times$ 2 temporal phases + 1 global parameter.

7. Readout. Widefield fluorescence microscopy with sCMOS camera (100+ fps for fast oscillations). Simultaneous multi-channel imaging via spectral unmixing or sequential filter switching. Boundary signals measured as fluorescence intensity in annular ROIs at vesicle periphery.

8. Predicted observables.

- Vesicles in same environment converge to same boundary oscillation pattern (code)
- Different environments produce distinguishable patterns (separation ratio >10×)
- Removing substrate competition (single reporter) collapses code diversity
- Intermediate coupling strength maximizes code discriminability

Estimated setup cost: \$50–100K for microfluidics, fluorescence microscope, and environmental control. Timeline: 6–12 months to first reproducible code emergence demonstra-

tion.

9. The messy version (recommended). The clean protocol above is conservative—it uses well-characterized components for experimental control. But our framework predicts that code emergence should be *more* robust under high-dimensional prebiotic conditions, not less. To test this directly:

- Replace defined lipids with Miller-Urey tar or meteoritic organic extracts
- Use formose reaction mixtures (autocatalytic sugar synthesis) instead of single oscillators
- Add random peptide libraries or prebiotic amino acid mixtures
- Let membrane composition self-assemble from heterogeneous amphiphile pools

If codes emerge from this chemical mess—and our theory says they should—that is far stronger evidence than emergence from a clean BZ system. The prediction is counterintuitive: *more chemical species → higher effective dimensionality → stronger substrate competition → sharper discretization.* The messy experiment is the real test.

What Would Falsify This Framework?

- Removing substrate competition ($h = 1$) should collapse code capacity → *confirmed* (Table, Section 4)
- Removing temporal cycles should reduce code diversity → *confirmed* (separation ratio $> 300\times \rightarrow < 50\times$)
- Code separation should peak at intermediate coupling → *confirmed* (Figure 2C)
- Predator size should track N_{ceiling} across parameter sweeps → *confirmed* (Table, Section 8)
- Lewis games should produce equivalent codes without substrate competition → *confirmed* (Section 5)
- **Open prediction**: Coupled vesicle arrays with oscillatory chemistry should spontaneously develop reproducible discrete boundary states

9.7 Limitations

Several limitations constrain interpretation of these results:

Simulation without experimental validation. This work presents computational proof-of-concept, not experimental demonstration. The framework generates testable predictions—coupled vesicle arrays should develop reproducible discrete boundary states—but these predictions remain untested.

Phenomenological dynamics. The reservoir model (echo state network with tanh nonlinearity and spectral radius 0.92) is a generic proxy for high-dimensional reaction networks, not literal chemistry. We claim that three features are invariant to replacing it with explicit chemical reaction networks: (1) the substrate competition discretizer (Eq. 1), which maps continuous concentrations to winner-take-most outputs via any saturating kinetics; (2) the coupling topology constraint, which forces coordination through shared boundaries; and (3) the observability limitation, which restricts inter-compartment information to low-dimensional boundary signals regardless of internal complexity. Future work should im-

plement explicit chemical kinetics, potentially building on established protocell simulation platforms [6], to verify this invariance claim.

What we explain vs. what we don't. Our model explains why degeneracy is adaptive (basin-robustness correlation), why codes emerge (coordination pressure), and why ecological differentiation occurs (coherence costs). It does **not** explain the specific structure of the genetic code—why degeneracy concentrates at position 3, why certain amino acids have more codons than others, or why the code has error-correcting geometry. These require chemistry (tRNA structure, ribosome mechanics) not just dynamics.

Lewis game scale. Our Lewis signaling validation used 4–8 states. Scaling to 64 states (matching the genetic code) may reveal additional constraints or failure modes.

P-adic connection is correlational. The p-adic distance predicts synonymy ($r = 0.26$), but this does not prove the genetic code was *generated* by p-adic dynamics. It may simply be that error-correcting codes generically have this structure.

10 Conclusion

We have shown that symbolic codes emerge generically from coordination pressure in coupled compartment networks. Two independent approaches—physical substrate competition and abstract Lewis signaling games—produce equivalent results, demonstrating that code emergence is robust across mechanisms.

The codes that emerge have structure matching the genetic code: degeneracy correlates with robustness ($r = 0.80 \pm 0.08$, $n = 20$), and p-adic distance predicts synonymy. However, our model explains the *function* of degeneracy (noise absorption) but not its *form* (concentration at position 3). A complete theory requires both dynamics and chemistry.

Metabolic ceilings on coherence prevent homogenization and generate predator-prey dynamics without specialized machinery. If correct, ecological differentiation may predate genetic encoding—arising from physics before biology.

Code availability: `https://github.com/todd866/protocell-codes`
Companion papers: Extended mathematical foundations in [13, 15].

Declarations

Funding

This research received no external funding.

Competing Interests

The author declares no competing interests.

Author Contributions

Ian Todd conceived the theoretical framework, designed and implemented the simulations, performed the analysis, and wrote the manuscript.

Data Availability

All simulation code and data required to reproduce the results are available at `https://github.com/todd866/protocell-codes`. No experimental datasets were generated.

Code Availability

The simulation code is open source under MIT license: `https://github.com/todd866/protocell-codes`

Ethics Approval

Not applicable. This study involves computational simulations only; no human participants, animal subjects, or biological materials were used.

References

[1] J. W. Szostak, D. P. Bartel, and P. L. Luisi. Synthesizing life. *Nature*, 409:387–390, 2001.

[2] M. W. Powner, B. Gerland, and J. D. Sutherland. Synthesis of activated pyrimidine ribonucleotides in prebiotically plausible conditions. *Nature*, 459:239–242, 2009.

[3] J. D. Sutherland. The origin of life—out of the blue. *Angewandte Chemie International Edition*, 55:104–121, 2016.

[4] I. A. Chen and P. Walde. From self-assembled vesicles to protocells. *Cold Spring Harbor Perspectives in Biology*, 2:a002170, 2010.

[5] D. A. Baum, Z. Peng, E. Dolson, E. Smith, A. M. Plum, and P. Gagrani. The ecology–evolution continuum and the origin of life. *Journal of the Royal Society Interface*, 20:20230346, 2023.

[6] B. Shirt-Ediss, A. Ferrero-Fernández, D. De Martino, L. Bich, A. Moreno, and K. Ruiz-Mirazo. Modelling the prebiotic origins of regulation and agency in evolving protocell ecologies. *Philosophical Transactions of the Royal Society B*, 380:20240287, 2025.

[7] Z. Peng, A. M. Plum, P. Gagrani, and D. A. Baum. An ecological framework for the analysis of prebiotic chemical reaction networks. *Journal of Theoretical Biology*, 507:110451, 2021.

[8] R. A. Black, M. C. Blosser, B. L. Stottrup, R. Tavakley, D. W. Deamer, and S. L. Keller. Nucleobases bind to and stabilize aggregates of a prebiotic amphiphile, providing a viable mechanism for the emergence of protocells. *Proceedings of the National Academy of Sciences*, 110:13272–13276, 2013.

[9] O. Markovitch and D. Lancet. Horizontal transfer of code fragments between protocells can explain the origins of the genetic code without vertical descent. *Scientific Reports*, 8:1–12, 2018.

[10] M. Shirt-Ediss, R. V. Solé, and K. Ruiz-Mirazo. Prebiotic vesicle formation and the necessity of salts. *Origins of Life and Evolution of Biospheres*, 45:133–145, 2015.

[11] T. Froese, N. Virgo, and T. Ikegami. Behavioral metabolution: The adaptive and evolutionary potential of metabolism-based chemotaxis. *Origins of Life and Evolution of Biospheres*, 49:245–277, 2019.

[12] A. Pohorille and K. Schweighofer. Toward understanding protocell mechanosensation. *Origins of Life and Evolution of Biospheres*, 41:435–447, 2011.

[13] I. Todd. Constraint exchange as manifold expansion: Communication beyond information in high-dimensional systems. Preprint, 2026. Available: `https://github.com/todd866/manifold-expansion/blob/main/constraint_exchange.pdf`

[14] I. Todd. Intelligence as high-dimensional coherence: The observable dimensionality bound and computational tractability. Under review, *BioSystems*, 2026.

[15] I. Todd. Curvature amplification of tracking complexity on statistical manifolds. Preprint, 2026. Available: `https://github.com/todd866/tracking-complexity/blob/main/geodesic_separation.pdf`

[16] C. R. Woese. *The Genetic Code: The Molecular Basis for Genetic Expression*. Harper & Row, New York, 1967.

[17] M. Yarus, J. J. Widmann, and R. Knight. RNA–amino acid binding: A stereochemical era for the genetic code. *Journal of Molecular Evolution*, 69:406–429, 2009.

[18] F. H. C. Crick. The origin of the genetic code. *Journal of Molecular Biology*, 38:367–379, 1968.

[19] J. T.-F. Wong. A co-evolution theory of the genetic code. *Proceedings of the National Academy of Sciences*, 72:1909–1912, 1975.

[20] S. J. Freeland and L. D. Hurst. The genetic code is one in a million. *Journal of Molecular Evolution*, 47:238–248, 1998.

[21] S. M. Secor and H. V. Carey. Integrative physiology of fasting. *Comprehensive Physiology*, 6:773–825, 2016.

[22] S. A. Benson-Amram, B. Dantzer, G. Stricker, E. M. Swanson, and K. E. Holekamp. Brain size predicts problem-solving ability in mammalian carnivores. *Proceedings of the National Academy of Sciences*, 113:2532–2537, 2016.

[23] K. E. Holekamp and S. A. Benson-Amram. The evolution of intelligence in mammalian carnivores. *Interface Focus*, 7:20160108, 2017.

[24] A. Cavagna, A. Cimarelli, I. Giardina, G. Parisi, R. Santagati, F. Stefanini, and M. Viale. Scale-free correlations in starling flocks. *Proceedings of the National Academy of Sciences*, 107:11865–11870, 2010.

[25] A. E. Ross and D. R. McKenzie. Predator-prey dynamics in a complex plasma. *Scientific Reports*, 6:29618, 2016.

[26] C. H. Meredith, P. G. Moerman, J. Groenewold, et al. Predator-prey interactions between droplets driven by non-reciprocal oil exchange. *Nature Chemistry*, 12:1136–1142, 2020.

[27] N. Horibe, M. Hanczyc, and T. Ikegami. Mode switching and collective behavior in chemical oil droplets. *Entropy*, 13:709–719, 2011.

[28] C. C. Grueter, B. Chapais, and D. Zinner. Evolution of multilevel social systems in nonhuman primates and humans. *International Journal of Primatology*, 33:1002–1037, 2012.

[29] Z. Huang, X. Qi, C. C. Grueter, P. A. Garber, S. Guo, and B. Li. Multilevel societies facilitate infanticide avoidance through increased extrapair matings. *Animal Behaviour*, 161:127–137, 2020.

[30] J. Jiang, Z. Liu, H. Chen, and M. Crossley. Mimicking lightning-induced electrochemistry on the early Earth. *Proceedings of the National Academy of Sciences*, 121(32):e2400819121, 2024.

[31] S. A. Kauffman. *The Origins of Order: Self-Organization and Selection in Evolution*. Oxford University Press, New York, 1993.

[32] M. Eigen. Selforganization of matter and the evolution of biological macromolecules. *Die Naturwissenschaften*, 58:465–523, 1971.

[33] H. R. Maturana and F. J. Varela. *Autopoiesis and Cognition: The Realization of the Living*. D. Reidel Publishing Company, Dordrecht, 1980.

[34] D. Deamer. The role of lipid membranes in life's origin. *Life*, 7:5, 2017.

[35] E. Branscomb and M. J. Russell. Turnstiles and bifurcators: The disequilibrium converting engines that put metabolism on the road. *Biochimica et Biophysica Acta (BBA)—Bioenergetics*, 1827:62–78, 2013.

[36] W. Hordijk and M. Steel. Detecting autocatalytic, self-sustaining sets in chemical reaction systems. *Journal of Theoretical Biology*, 227:451–461, 2004.

[37] D. K. Lewis. *Convention: A Philosophical Study*. Harvard University Press, Cambridge, MA, 1969.

[38] B. Skyrms. *Signals: Evolution, Learning, and Information*. Oxford University Press, Oxford, 2010.

[39] E. Yurova Axelsson and A. Khrennikov. Universal dynamical function behind all genetic codes: P-adic attractor dynamical model. *BioSystems*, 246:105353, 2024.

[40] A. U. Igamberdiev. Foundations of metabolic organization: Coherence as a basis of computational properties in metabolic networks. *BioSystems*, 50:1–16, 1999.

[41] A. U. Igamberdiev. Biological thermodynamics: Ervin Bauer and the unification of life sciences and physics. *BioSystems*, 235:105089, 2024.

[42] B. Dragovich, A. Y. Khrennikov, and S. V. Kozyrev. p-Adic mathematics and theoretical biology. *BioSystems*, 199:104288, 2021.

[43] B. Dragovich, A. Y. Khrennikov, and N. Ž. Mišić. p-Adic hierarchical properties of the genetic code. *BioSystems*, 185:104017, 2019.

[44] N. Takeuchi and K. Kaneko. The origin of the central dogma through conflicting multilevel selection. *Proceedings of the Royal Society B*, 286:20191359, 2019.

A Mathematical Derivation: Predator-Prey from Coherence Constraints

This appendix derives predator-prey dynamics from minimal physical assumptions using coherence constraints and superlinear maintenance costs.

Assumptions:

- Units maintain internal coherence against thermal noise (cost scales with dimensionality)
- Resource acquisition scales linearly with effective dimensionality
- Evolutionary dynamics with absorbing boundary at $D = 0$ (loss of coherence is irreversible on short timescales)
- Coupling between units allows asymmetric destabilization (high-D can perturb low-D)
- Population-level selection proportional to net fitness

A.1 Coherence Cost Framework

Consider a population of N dynamical units (protocells, droplets, plasma regions) that must maintain internal coordination against thermal noise. Let D_i denote the effective dimensionality of unit i. The **coherence maintenance cost** is:

$$C(D_i) = \alpha D_i^{\gamma} \quad \text{with } \gamma > 1 \tag{13}$$

where $\alpha > 0$ is a rate constant and $\gamma > 1$ captures superlinear scaling. The exponent $\gamma > 1$ reflects that maintaining coherence across D degrees of freedom requires suppressing $\binom{D}{2} = O(D^2)$ pairwise decoherence channels.

Units acquire resources from a shared environment at rate $A(D_i, R) = \beta D_i R$, where R is resource concentration. Linear scaling with D_i reflects that more complex units exploit more resource types.

A.2 Generic Bistability (Proposition 1)

Proposition. Under coherence constraints with $\gamma > 1$, populations evolve toward a bimodal distribution with attractors at $D_L \approx 0$ (minimal coherence) and D_H satisfying the first-order condition.

Sketch. Net fitness is $F(D, R) = \beta DR - \alpha D^\gamma$. Setting $\partial F/\partial D = 0$ yields $D^* = (\beta R/\alpha\gamma)^{1/(\gamma-1)}$. Since $\partial^2 F/\partial D^2 < 0$, this is a maximum. But $F(0) = 0$, so both $D = 0$ and $D = D^*$ are stable under stochastic population dynamics.

This bistability is the origin of ecological differentiation: units at $D \approx D^*$ become "predators" (high-D, high-cost); units at $D \approx 0$ become "prey" (low-D, low-cost).

A.3 The Extraction Operator (Proposition 2)

Proposition. If high-D units can destabilize low-D units through coupling, extraction emerges generically.

Proof sketch. High-D units have higher resource acquisition, more control degrees of freedom, and lower relative noise sensitivity. Low-D units' coherence depends on maintaining a narrower set of correlations. Under shared resource depletion or perturbation, low-D units lose coherence first. Upon decoherence, released matter/energy becomes available as a resource gradient that high-D units capture preferentially. This asymmetric vulnerability produces net flow from low-D to high-D populations. □

A.4 Derivation of Lotka-Volterra (Proposition 3)

Proposition. Under coherence constraints with extraction, population dynamics take Lotka-Volterra form:

$$\dot{x}_1 = x_1[\alpha_1 - \beta_{12} x_2] - k x_1^n \tag{14}$$

$$\dot{x}_2 = x_2[-\gamma_2 + \delta_{21} x_1] \tag{15}$$

where x_1 is prey density, x_2 is predator density, and the nonlinear loss term kx_1^n with $n > 1$ arises from intraspecific competition.

Sketch. Prey dynamics: growth when acquisition exceeds cost, decline under predation and crowding. Predator dynamics: high coherence costs offset by extraction. The nonlinear loss with $n > 1$ reflects superlinear coherence costs under crowding.

Remark. Without the nonlinear loss term ($k = 0$ or $n = 1$), the system exhibits neutrally stable orbits. Stable limit cycles require $n > 1$, reflecting the physical necessity of superlinear coherence costs.

A.5 Connection to Experiments

Dusty plasmas [25]: Electrons (prey) and dust grains (predators) exhibit Lotka-Volterra oscillations. The authors find $n \approx 2$ required for stability, confirming our prediction that $\gamma = 2$ (pairwise decoherence) maps to $n = 2$.

Chemotactic droplets [26]: BOct droplets (predator) chase EFB droplets (prey) via micelle-mediated oil transport. The predator exhibits higher coherence—directed pursuit requires maintaining interfacial gradients against diffusion. The prey shows lower coherence (passive repulsion). This asymmetry in behavioral dimensionality matches our framework precisely.

Mode-switching droplets [27]: Four behavioral modes correspond to different effective dimensionalities. Transitions reflect coherence threshold crossings under noise.

A.6 General Principle

Any system satisfying (1) coherence maintenance with superlinear cost, (2) resource competition with linear acquisition, and (3) coupling between units of different dimensionality will generically exhibit predator-prey dynamics. Evolution elaborates this pre-existing scaffold; it does not create it.